Robust Dental Arch Curve Optimization Using a Standard Arch Form for Panoramic Reconstruction

Songze Zhang[1,2][0000−0003−4548−4363], Benxiang Jiang[1,2][0000−0001−5135−7630], Jingyi Lyu[1,2][0009−0005−4822−8877], and Hongjian Shi[1,2,*][0000−0001−8732−4101]

[1] Guangdong Provincial Key Laboratory of Interdisciplinary Research and Application for Data Science, Beijing Normal-Hong Kong Baptist University, Zhuhai, 519087, China shihj@uic.edu.cn

[2] Hong Kong Baptist University, Hong Kong, 999077, China

Abstract. This study presents a robust dental arch curve optimization method for panoramic image reconstruction from CBCT images. The proposed approach integrates prior maxillofacial anatomical knowledge through a statistical standard arch form and introduces an assessment function to guide the fitting of anatomically accurate and convex dental arch curves. Experimental validation in clinically diverse CBCT datasets demonstrates the effectiveness of the method in challenging scenarios, including orthodontic appliances, rigid internal fixation, mixed dentition, complete edentulism, and impacted teeth. The results confirm that the proposed method enables high-quality panoramic image reconstruction suitable for various dental imaging applications.

Keywords: Dental arch· Panoramic imaging · Polynomial curve fitting · CBCT.

1 Introduction

Cone-beam computed tomography (CBCT) provides high-resolution imaging of intraoral and maxillofacial structures and has become increasingly prevalent in dental clinical practice [1]. In contrast, panoramic radiography has been widely used for decades, offering a convenient overview of the entire maxillofacial region in a single image [2]. These two modalities are often used in combination for diagnosis and treatment planning. Reconstructing panoramic images from CBCT volumes enables extraction of both 3D and 2D information from a single scan, thereby reducing patient radiation exposure [3].

Since panoramic reconstruction involves projecting the 3D CBCT volume onto a plane defined by the dental arch curve, the accuracy of dental arch curve detection is critical to the quality of the reconstructed panoramic image. A common strategy involves generating an axial maximum intensity projection (MIP) of the tooth crown slices, segmenting the teeth and jawbone, refining the segmentation mask, and fitting the dental arch curve using splines or polynomial

interpolation over sampled points [4–6]. While these methods are straightforward and computationally efficient, they typically ignore the geometric convexity of the dental arch and fail to incorporate prior anatomical knowledge of maxillofacial structures. Moreover, existing approaches are rarely validated on clinically complex cases such as orthodontic appliances, rigid internal fixation, mixed dentition, complete edentulism, or impacted teeth.

In this study, we propose a dental arch curve optimization method based on a statistical standard arch form [7], which integrates prior knowledge of typical maxillofacial anatomy. An assessment function is introduced to guide the optimization process, ensuring that the resulting curve is both anatomically accurate and geometrically convex. The proposed method enables robust and high-quality panoramic image reconstruction across a wide range of clinically challenging CBCT datasets.

2 Method

2.1 Overview

This section describes our dental arch optimization method based on a standard form for robust panoramic image reconstruction from CBCT images. The process begins by identifying the axial range that includes the tooth crowns. Based on this range, MIP images of the crowns and mandible are generated. A standard dental arch curve is then fitted to the jawbone structures visible in these MIP images. Subsequently, the curve is further optimized using the standard form as a prior, and the resulting dental arch is employed for panoramic image reconstruction. This method detects accurate dental arch curves across diverse CBCT datasets.

2.2 Axial MIP Image Generation

Generating the axial MIP image from a carefully selected stack of axial slices significantly improves the accuracy of dental arch curve detection. The selected range should primarily include the tooth crowns. If the MIP image is generated from all axial slices, it introduces redundant bone structures surrounding the dental arch, which impairs curve detection, as illustrated in Fig. 1(a). Inspired by the axial MIP generation method in [4], we propose an axial MIP image generation method for dental arch curve optimization.

Oral CBCT images mainly consist of three tissue types: air, soft tissue, and bone. We apply K-means clustering with $k = 3$ on the coronal MIP image (Fig. 2(a) and (d)) to segment these regions. Since tooth crowns exhibit higher intensity than other bony structures, we select the intensity value at the bone cluster center as the threshold for crown segmentation. This yields the tooth crown masks shown in Fig. 2(b) and (e). To identify the axial range containing crowns, we count the number of crown pixels in each row to construct a histogram (blue bars in Fig. 2(c) and (f)). A Gaussian Mixture Model (GMM) is then used

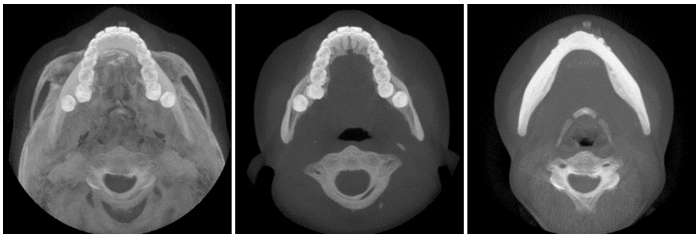

Fig. 1. From left to right: (a) the axial MIP image of all slices; (b) the axial MIP image of tooth crowns; (c) the axial MIP image of mandible below the tooth crowns.

to fit the histogram. To determine the optimal number of GMM components, we test models with 1 to $K_{max} = 5$ components and evaluate each using the Bayesian Information Criterion (BIC):

$$\mathrm{BIC} = p \ln N - 2 \ln L, \tag{1}$$

where p is the number of model parameters, N is the number of data points, and L is the model likelihood. Although, the BIC penalizes complexity via the $p \ln N$ term, we observed that the models with $K_{\max}$ components often yield the lowest BIC, suggesting under-penalization. Therefore, we introduce a modified BIC, BIC_{mod}, to more strongly penalize complex models:

$$\mathrm{BIC}_{mod} = \alpha p \ln N - 2 \ln L, \tag{2}$$

where $\alpha > 1$ could increase the penalty for additional parameters, helping to avoid overfitting and $\alpha = 20$ in the experiments. The GMM with the lowest BIC_{mod} is selected as the fitted histogram model, as the red curves depicted in Fig. 2(c) and (f).

Let μ_h, α_h and p_h denote the mean, standard deviation, and peak value of the dominant component. If no other component within $[\mu_h - 3\sigma_h, \mu_h + 3\sigma_h]$ exceeds $0.8\,p_h$, then this range defines the axial slices range of tooth crown: $[R_s, R_e] = [\mu_h - 3\sigma_h, \mu_h + 3\sigma_h]$, shown by green lines in Fig. 2(b). Otherwise, if two prominent components are detected, as in Fig. 2(f), we denote their statistics as (μ_{up}, σ_{up}) and $(\mu_{low}, \sigma_{low})$. The tooth crown-containing slice range is defined as: $[R_s, R_e] = [\mu_{up} - 3\sigma_{up}, \mu_{low} + 3\sigma_{low}]$ as the green lines in Fig. 2(e). Based on the determined slice range, two axial MIP images are generated: one from $[R_s, R_e]$, representing the tooth crowns, and the other from $[R_e + 1, end]$, representing the mandible below the crowns, as shown in Fig. 1(b) and (c), respectively. Here, *end* denotes the index of the bottom axial slice. These two MIP images are used for standard dental arch curve fitting as follows.

2.3 Standard Dental Arch Curve Fitting

The dental arch represents the anatomical layout of the dentition and jaw. Based on population statistics, Welander et al. [7] configured a standard dental arch

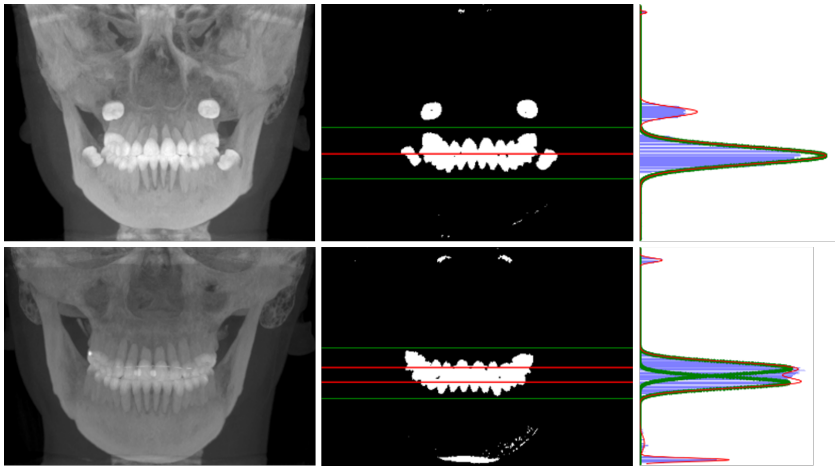

Fig. 2. From top to the bottom, left to right: (a) the coronal MIP image; (b) corresponding crown mask, red line shows the center of the dominant GMM component in (c), green lines indicate axial slice range containing crowns; (c) histogram of crown pixels (blue bars), red curve is GMM fit, green curve is the dominant component; (d)-(f) are analogous results for another dataset with two prominent GMM components.

form composing a dentition curve y_D and a mandible curve y_M, defined as:

$$y_D = d_2x^2 + d_4x^4, \tag{3}$$

$$y_M = m_0 + m_2x^2 + m_4x^4 + m_6x^6, \tag{4}$$

with coefficients $d_2 = -0.014097$ and $d_4 = -7.3814 \times 10^{-5}$, $m_0 = -5.4341$,$m_2 = -0.040436$, $m_4 = 1.0507 \times 10^{-5}$, $m_6 = -2.7483 \times 10^{-9}$, units are millimeter (mm).

These curves characterize the standard morphology of the dentition and mandible and must be spatially aligned to individual CBCT datasets. Alignment is performed using two axial MIP images: one representing the tooth crowns (Fig. 1(b)) and the other representing the mandible region below the crowns (Fig. 1(c)). Jawbone structures are segmented from these images as follows:

1. The axial MIP images are first denoised using a Gaussian filter.
2. K-means clustering with $k = 3$ is applied to classify pixels into bone, soft tissue, and air; the bone cluster is retained.
3. The largest connected component is extracted and smoothed via morphological operations to generate jawbone masks (Fig. 3(a) and (b)).

To locate the highest points on the jawbone, we analyze the central 10 mm column of each axial MIP image. The upmost jaw bones points from top to bottom and from bottom to top in the central 10 mm are identified. These may include multiple local maxima on each side, shown as green points in Fig. 3(a) and (b). The mean coordinates of upmost points in top and bottom sides are

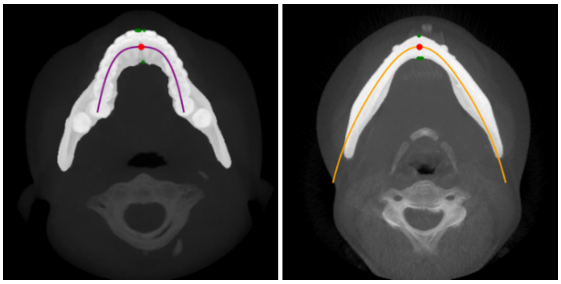

Fig. 3. Superimposing images (white masks represent the segmented jawbones) from left to right: (a) jawbone mask from Fig. 1(b); (b) jawbone mask from Fig. 1(c)

computed, and the average of these means defines the vertex of each standard curve (shown as red points). Using these vertex points, the standard dentition and mandible curves are spatially shifted and overlaid as the purple and orange curves in Fig. 3.

The shifted curves serve as the initial representations of the individual's dentition and mandible geometry. To obtain a unified initial standard dental arch curve, these two curves are fused using a smooth blending function. A window function $W(x)$ is defined as:

$$W(x) = [\frac{x-a}{b-a}]^4, x \in [a,b], a < b. \tag{5}$$

Let $P_L = (x_{PL}, y_{PL})$ and $P_R = (x_{PR}, y_{PR})$ denote the leftmost and rightmost intersections between the dentition and mandible curves. Let $V_M = (x_{VM}, y_{VM})$ be the vertex of the mandible curve, and $R_D = 42\,mm$ be the half horizontal span of the dentition curve. The piecewise initial standard dental arch curve $C_S(x)$ is then defined as:

$$C_S(x) = \begin{cases} C_M(x), & x < x_{VM} - R_D \\ W(x)C_D(x) + \big[1 - W(x)\big]C_M(x), & x_{VM} - R_D \le x \le x_{PL} \\ C_D(x), & x_{PL} < x < x_{PR} \\ W(-x)C_D(x) + \big[1 - W(-x)\big]C_M(x), & x_{PR} \le x \le x_{VM} + R_D \\ C_M(x), & x > x_{VM} + R_D \end{cases} \tag{6}$$

where $C_D(x)$ and $C_M(x)$ are the shifted dentition and mandible curves, as the purple and orange curve shown in Fig. 4(a). The initialized standard dental arch curve is optimized to fit the individual dataset in following step.

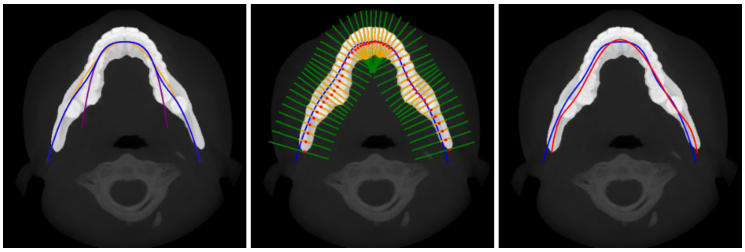

Fig. 4. Jawbone masked axial MIP image of tooth crowns from left to right: (a) the blue curve is the initial standard dental arch; purple and orange curves are the shifted dentition and mandible curves; (b) green lines represent perpendiculars to the blue curve, their intersections with jawbone masks (orange segments) define central points (red); (c) red curve shows the optimized dental arch.

2.4 Dental Arch Curve Optimization

The initial standard dental arch curve serves as a prior template and must be adapted to the individual's jawbone morphology. To achieve this, we extract central points of the jawbone from the axial MIP image of the tooth crown slices. Perpendicular lines are drawn at each point along the initial standard dental arch curve (green lines in Fig. 4(b)). Each perpendicular intersects the segmented jawbone mask, producing intersection segments (orange lines in Fig. 4(b)). The center of each segment is computed by averaging the coordinates of its endpoints, forming a set of central points (red dots in Fig. 4(b)). While Fig. 4(b) shows sampled lines for visualization, in practice, perpendiculars are generated at every point along the initial curve to obtain a dense set of central points.

These points are then used to fit a new dental arch curve using polynomial regression. However, the optimal polynomial degree varies across datasets and must balance accuracy, simplicity, and geometric stability. To address this, we adopt the following criteria:

1. Minimize the average distance between the fitted curve and the central points.
2. Use the lowest polynomial degree that satisfies criterion 1 to reduce overfitting.
3. Ensure the fitted curve is as convex as possible for anatomical plausibility.

To integrate these criteria, we define an assessment function that combines mean squared error (MSE), polynomial degree penalty, and convexity regularization:

$$\mathcal{L}(f_D) = \sum_{i=1}^{n} \left(y_i - f_D(x_i)\right)^2 + \beta D + \gamma \left(1 - r_{\text{convex}}\right), \tag{7}$$

where (x_i, y_i) are the coordinates of the i-th central points, n is the number of the central points, $f_D(x) = \sum_{j=0}^{D} a_j x^j$ is the D-degree polynomial model, r_{convex} is the proportion of the curve domain over which the second derivative

$f''_D(x) > 0$, and $\beta = 1.5$, $\gamma = 100$ are empirically chosen weighting factors. Polynomial models with degrees ranging from 2 to 20 are fitted to the central points, and the one yielding the lowest value of $\mathcal{L}(f_D)$ is selected as the optimized dental arch curve, shown as the red curve in Fig. 4(c).

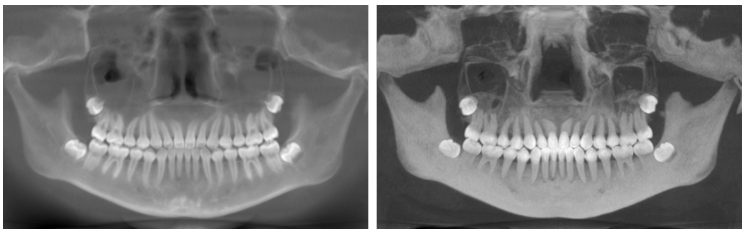

Fig. 5. From left to right: (a) ray-sum panoramic image; (b) MIP panoramic image.

Finally, panoramic images are reconstructed using the optimized dental arch curve with equal-arc-length sampling and a fixed arch thickness of 2 cm. Both ray-sum and MIP rendering techniques are applied to produce the final panoramic projections, as illustrated in Fig. 5.

3 Results

3.1 Datasets

This study utilized a partially open-access CBCT dataset released by Cui et al. [8–10], which comprises 150 CBCT volumes. Among these, 95 CBCT volumes include a complete dentomaxillofacial field of view (FOV). The remaining volumes contain either partial dentition and were therefore excluded from evaluation.

Given that panoramic images depict the full dentomaxillofacial structure, we used the 95 CBCT volumes to evaluate the proposed dental arch curve optimization method. These volumes include a wide range of clinically challenging cases commonly encountered in dentistry. Notably, some cases present multiple co-occurring conditions, including: orthodontic appliances (7 cases), mixed dentition (1 case), rigid internal fixation (9 cases), root canal (40 cases), crown restoration (49 cases), implants (36 cases), partial edentulism (74 cases), complete edentulism (2 cases) and impacted teeth (13 cases).

3.2 Experiment Results

In this study, panoramic images were reconstructed for all 95 CBCT volumes to validate the robustness of our proposed dental arch curve optimization method. The polynomial degree used for curve fitting was selected based on the assessment function defined in Eq. 7. Table 1 summarizes the distribution of the selected polynomial degrees.

Approximately 90% of the fitted dental arch curves were modeled using either 6th- or 8th-degree polynomials. This aligns with the design of the initial standard dental arch curve, which is formed by blending a 4th-degree dentition curve and a 6th-degree mandible curve, making a 6th- or 8th-degree polynomial generally sufficient for most cases. Additionally, most selected degrees were even, which may be attributed to their geometric suitability for producing convex-shaped curves.

Table 1. Statistical analysis of polynomial fitting degrees

Degree	6	8	9	12	14	**Total**
Number	26	58	2	6	3	95
Rate	27.37%	61.05%	2.10%	6.32%	3.16%	100%

The proposed method demonstrated well performance across various complex clinical scenarios. It effectively identified individualized dental arch curves and enabled high-quality panoramic image reconstruction. While Fig. 5 displays a case involving impacted teeth, Fig. 6 showcases four additional representative examples. In each case, the first column shows jawbone-masked axial MIP images of the crown slice, where the blue and red curves denote the initial standard and optimized dental arch curves, respectively. The second column presents the corresponding ray-sum panoramic images. These four cases cover a broad range of clinical challenges:

1. Orthodontic appliances and rigid internal fixation (1st row);
2. Mixed dentition with impacted teeth (2nd row);
3. Rigid internal fixation, dental implants, and partial edentulism (3rd row);
4. Complete edentulism with root canal treatment and crown restorations (4th row).

Despite the anatomical complexity in these examples, the reconstructed panoramic images retain high anatomical fidelity. These results suggest that the proposed method generalizes well to diverse and challenging clinical conditions, demonstrating notable robustness and adaptability.

4 Conclusions

This paper presents a dental arch curve optimization method that incorporates prior maxillofacial anatomical knowledge through a standard arch form. An assessment function is designed to guide the fitting process, ensuring anatomically accurate and convex dental arch curves. The proposed method exhibits strong robustness and accuracy across a wide range of clinically challenging CBCT cases and enables high-quality panoramic image reconstruction. These results highlight the method's potential for reliable application in dental imaging and treatment planning.

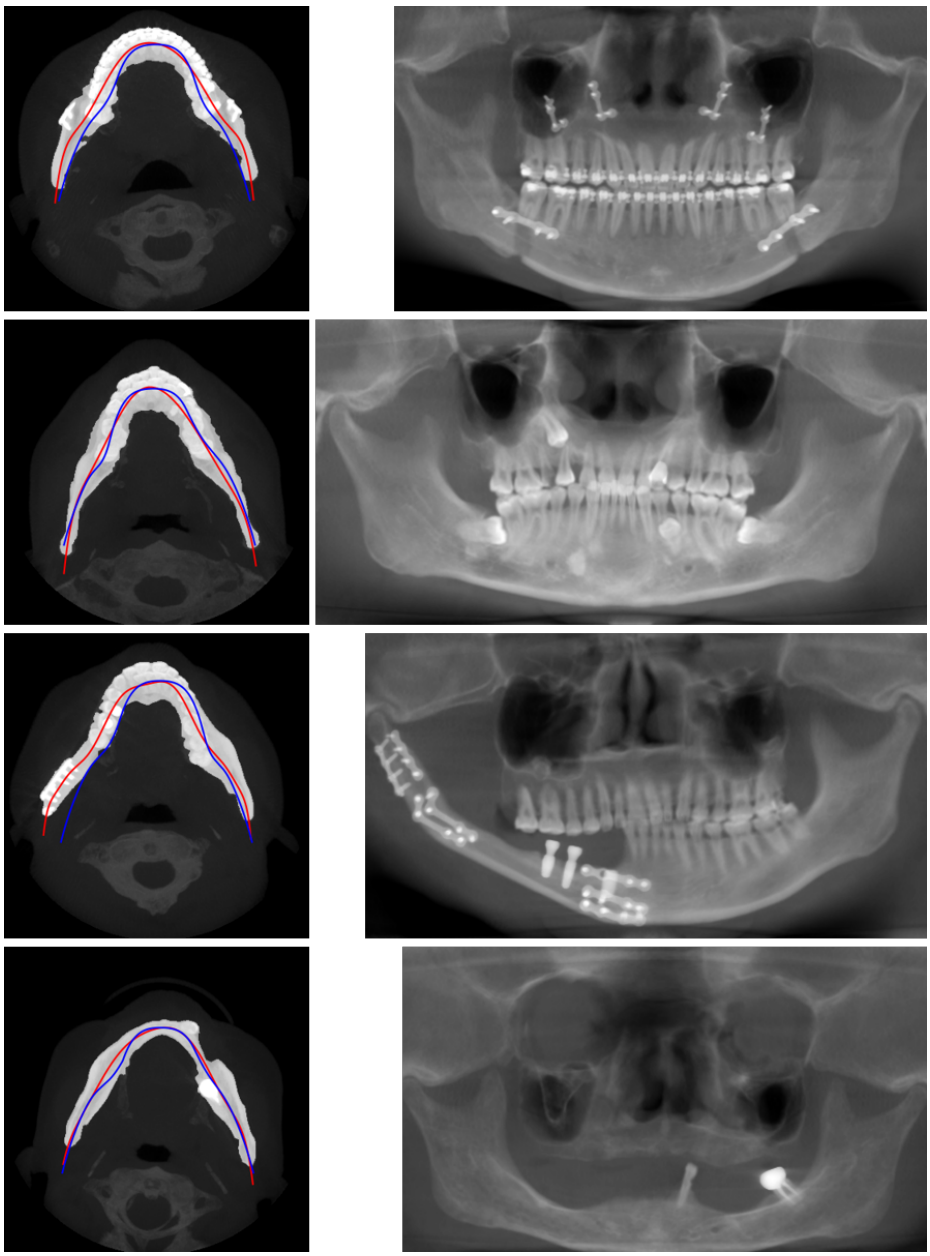

Fig. 6. The optimized dental arch curves (the first column) and the corresponding ray-sum panoramic images of four complex cases (the second column). *Note that the panoramic images have varying widths because the lengths of the detected dental arch curves differ.*

Acknowledgments. This work was supported in part by the Guangdong Higher Education Key Platform and Research Project under Grant 2020ZDZX3039, in part by the Guangdong Provincial Key Laboratory of Interdisciplinary Research and Application for Data Science under Grant 2022B1212010006.

References

1. Scarfe, W.C., Farman, A.G.: What is Cone-Beam CT and How Does it Work? Dental Clinics of North America **52**, 707–730 (2008)
2. Ameli, N., Miri Moghaddam, M., Lai, H., Pacheco-Pereira, C.: Automated quality evaluation of dental panoramic radiographs using deep learning. Imaging Science in Dentistry **55**, (2025)
3. Zhang, S., Jiang, B., Shi, H.: Dental Arch Curve Optimization from Standard Dental Arch Curves. In: 2nd International Conference on Pattern Recognition, Machine Vision and Intelligent Algorithms (PRMVIA), pp. 98–102 (2024)
4. Yun, Z., Yang, S., Huang, E., Zhao, L., Yang, W., Feng, Q.: Automatic reconstruction method for high-contrast panoramic image from dental cone-beam CT data. Computer Methods and Programs in Biomedicine **175**, 205–214 (2019)
5. Oliveira, L.A.V., Moran, M.B.H., Faria, M.D.B., Bastos, L.F., Giraldi, G., Da Rosa, L.A.R., Neto, J.F.N., Conci, A.: Dental arch definition in computed tomographs using two semi-automatic methods. Medical & Biological Engineering & Computing **60**, 3499–3508 (2022)
6. Zhang, J., Jiang, Y., Gao, F., Zhao, S., Yang, F., Song, L.: A Fast Automatic Reconstruction Method for Panoramic Images Based on Cone Beam Computed Tomography. Electronics **11**(15), 2404 (2022)
7. Welander, U., Nummikoski, P., Tronje, G., McDavid, W.D., Legrell, P.E., Langlais, R.P.: Standard forms of dentition and mandible for applications in rotational panoramic radiography. Dentomaxillofacial Radiology **18**, 60–67 (1989)
8. Cui, Z., Fang, Y., Mei, L., Zhang, B., Yu, B., Liu, J., Jiang, C., Sun, Y., Ma, L., Huang, J., Liu, Y., Zhao, Y., Lian, C., Ding, Z., Zhu, M., Shen, D.: A fully automatic AI system for tooth and alveolar bone segmentation from cone-beam CT images. Nature Communications **13**, 2096 (2022)
9. Cui, Z., Li, C., Wang, W.: ToothNet: Automatic Tooth Instance Segmentation and Identification From Cone Beam CT Images. In: IEEE/CVF Conference on Computer Vision and Pattern Recognition (CVPR), pp. 6361–6370 (2019)
10. Cui, Z., Zhang, B., Lian, C., Li, C., Yang, L., Wang, W., Zhu, M., Shen, D.: Hierarchical Morphology-Guided Tooth Instance Segmentation from CBCT Images. In: Information Processing in Medical Imaging (IPMI), pp. 150–162. Springer International Publishing (2021)